Available online at www.sciencedirect.com
SCIENCE DIRECT®
Journal of Sound and Vibration 274 (2004) 583–603
JOURNAL OF SOUND AND VIBRATION
www.elsevier.com/locate/jsvi

Discrimination of coupled structural/acoustic duct modes by active control: principles and experimental results ☆

V. Martin[a], A. Cummings[b,*], C. Gronier[c]

[a] *Laboratoire d'Électromagnétisme et d'Acoustique, École Polytechnique Fédérale de Lausanne, CH-1015 Lausanne, Switzerland*
[b] *Department of Engineering, University of Hull, Cottingham Road, East Yorkshire, Hull HU6 7RX, UK*
[c] *Laboratoire de Mécanique de Rouen, CNRS-INSA, Avenue de l'Université, BP08, 76801 St. Etienne du Rouvray Cedex, France*

Received 14 June 2002; accepted 29 May 2003

Abstract

The coupling of acoustic waves in an elastic-walled duct with structural waves in the wall(s), at low frequencies, gives rise to dispersive coupled structural/acoustic modes. Propagating coupled modes consist of a "fast wave", which propagates at all frequencies, together with "slow waves", which propagate above their "cut-on" frequencies. The fast wave is well known and has been experimentally observed many years ago. The lowest order slow wave has also been—indirectly—observed previously, though not independently of the fast wave. In this investigation, an identification technique involving a genetic algorithm and active control has permitted the separate visualization of the lowest order slow wave and the fast wave, in the case where these two modes coexist.

1. Introduction

In dynamics, problems involving structural/acoustic coupling have been tackled by various methods, from analytical modal descriptions of coupled wave motion to numerical methods including finite differences, finite elements and boundary elements. On the other hand, only a few characteristic physical phenomena have been well identified. Two of these are, first, alteration of the resonance frequencies of the two media considered separately (the structure alone and a

☆ Some of the material in this paper was presented at the Euro-Noise 2001 Conference at the University of Patras, Greece, 14–17 January 2001.

*Corresponding author. Tel.: +44-1482-465069; fax: +44-1482-466664.
E-mail address: a.cummings@hull.ac.uk (A. Cummings).

0022-460X/$ - see front matter
doi:10.1016/j.jsv.2003.05.021

rigid-walled acoustic cavity) and secondly, damping in the structure caused by acoustic radiation. Another physical phenomenon, in the case of guided waves, is associated with the particular nature of the coupling between the guided acoustic wave and the flexural motion in the walls of the waveguide. Here, the speed of the coupled wave system can be subsonic or supersonic, even for quasi-plane waves. Analytical models describing the effects of wall motion on guided acoustic waves have existed for several decades. Morse and Ingård [1], for example, give a good account of these effects. More recently, research on structural/acoustic coupling in ducts has involved both modelling (for example, in the work of Cabelli [2] and Martin and Vignassa [3]) and combinations of modelling and experimental observation (as in the work of Cummings [4] and Martin [5]). It has been shown theoretically [2–7] that there is a multiplicity of coupled structural/acoustic modes in both acoustically lined and unlined ducts, and that these modes are, in general, dispersive. Experimental data [4–7] are in agreement with these results. Gautier and Tahani [8] have demonstrated, both theoretically and experimentally, the existence of two structural/acoustic coupled waves in a circular rubber tube.

In general, more than one coupled mode can coexist and, even in experimental duct systems, a combination of propagating and evanescent coupled modes is usually present. One may ask whether each of these modes can be observed in isolation by the removal of others. This question also has relevance in a wider context, since coupled modes in which most of the mechanical power flow is in the structure (as opposed to the fluid) can play a role in flanking transmission mechanisms in dissipative duct silencers [9,10] and the removal of these modes from the vibroacoustic field in these devices could be a means of enhancing the acoustic performance.

In the present investigation, active control is applied to sound propagation in an experimental unlined duct with one flexible wall. The effort is concentrated on the removal of one or more coupled structural/acoustic waves. In this first investigation, the active control technique employed is similar to the original 1936 technique of Lueg, later termed "single channel feed-forward control" [11]. It is, in essence, a procedure by anticipation in the sense that the controller, the output of which is the driving signal to the secondary source intended to cancel the acoustic field, is totally predetermined on the basis of physical predictions of the result. There is no correction in the controller to improve the result after it has been observed, as there would be in a retroaction type such as the (by now) well-known auto-adaptive controller. The type of control used here has been analyzed recently in a simple configuration to test the adequacy of understanding of the entire electro-acoustic path [12].

In the first part of this paper, consideration is given to theoretical dispersion relationships for coupled waves, and the experimental arrangement is described. Some experimental data on a combination of two coupled waves are next presented, and the use of a genetic algorithm for the experimental determination of the amplitudes and phases of the two travelling wave components (in both directions along the duct axis) of each wave is described. The phase speed of each wave and its complex amplitude are thus found. The method of active control is implemented on the basis of these results, and each wave in turn is examined, the other being removed by the active control system. The results of this visualization technique are presented. The active control formulation is applied to structural waves in the flexible wall, but the secondary source—providing the "cancellation" signal—is acoustic.

2. A brief description of wave coupling

Since this investigation is mainly concerned with the experimental visualization of individual coupled modes by active control, the analysis of these modes will be presented rather briefly. This is done here in two parts. First, an approximate formulation, based on a variational technique, is given so that a simple analytical dispersion relationship may be obtained; this gives some physical insight into the problem. Secondly, a more accurate method is given, based on an exact solution of the structural equation of motion, leading to a dispersion relationship that gives predictions of sufficient accuracy for the purpose. Dispersion curves are given for the experimental duct.

2.1. Configuration of the experimental duct and establishment of an approximate dispersion relationship

The experimental duct was fabricated at the University of Hull, and was of rectangular cross-section, measuring 90 mm × 100 mm. It had three walls of 12 mm perspex, which were effectively rigid, and one wall (100 mm wide) of 0.6 mm aluminium plate, clamped along both edges, which was flexible. The duct is depicted in Fig. 1. One source loudspeaker was located at one end of the duct and another (on the lower, rigid, wall of the duct and not shown in Fig. 1) was situated about half-way along the length of the duct. A partially anechoic termination for both structural waves in the flexible wall and acoustic waves in the duct was located at the other end. A length of duct with all four walls rigid was placed between the source at the end of the duct and the beginning of the flexible duct wall. The flexible wall was clamped at the point where it met the abutting rigid wall. The transition between the rigid and flexible-walled duct sections was deliberately included so that a plane sound wave, incident from the rigid section, would generate a combination of

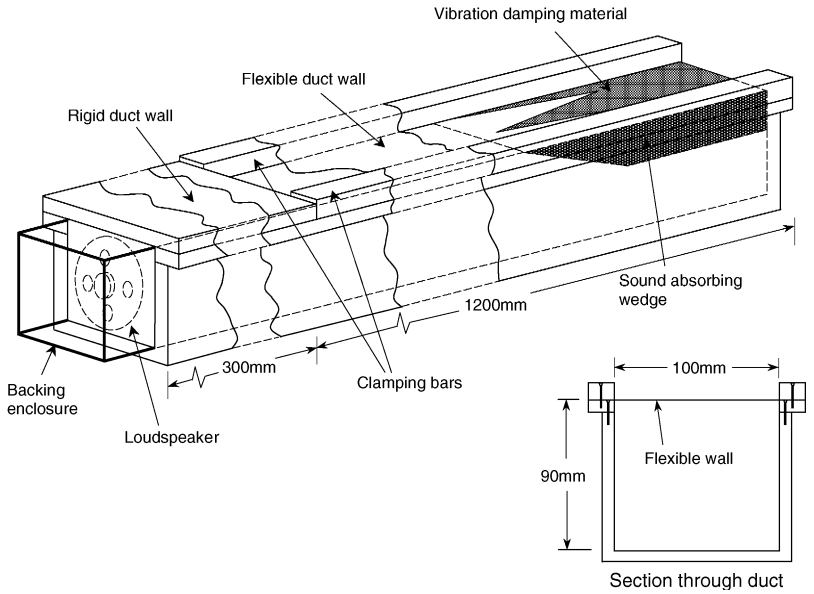

Fig. 1. The experimental duct.

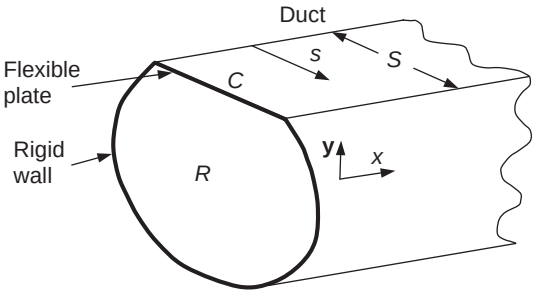

Fig. 2. A uniform duct consisting of a flat flexible plate mounted in rigid walls.

coupled structural/acoustic modes in the flexible-walled section. The effective width of the flexible wall was, because of the slightly rounded corners of the clamping bars, 107 mm rather than 100 mm.

An approximate dispersion relationship for a uniform duct with partly rigid and partly flexible walls may be established as follows. The geometry is shown in Fig. 2. It is assumed that the flexible part of the walls consists of a thin flat plate of width S. The axial co-ordinate is x and $\mathbf{y}$ is a position vector on the cross-section of the duct. On the cross-section, the region within the duct is denoted R and the flexible wall is denoted C in what follows. It will be assumed that a positive travelling coupled structural/acoustic mode propagates in the duct and plate, with a common axial wavenumber k_x. The sound pressure in R may be written as

$$p = P(\mathbf{y}) \exp[\mathrm{i}(\omega t - k_x x)] \tag{1a}$$

and the outward plate displacement as

$$u = U(s) \exp[\mathrm{i}(\omega t - k_x x)], \tag{1b}$$

s being a transverse co-ordinate on the plate. The acoustic wave equation in R and the equation of motion of the flexible wall may be written

$$\nabla_t^2 P + (k^2 - k_x^2)P = 0; \quad g[(d^2/\mathrm{d}s^2 - k_x^2)^2 U - k_p^4 U] = P_p(s), \tag{2a, b}$$

where ∇_t^2 is the Laplacian operator in two dimensions on the duct cross-section, k is the acoustic wavenumber ω/c, ω being the radian frequency and c the sound speed, k_p is the plate wavenumber, equal to $(m\omega^2/g)^{1/4}$, m and g are the mass/unit area and flexural rigidity of the plate and $P_p(s)$ is the amplitude of the interior/exterior acoustic pressure differential p_p forcing the plate motion, defined by $p_p = P_p(s)\exp[\mathrm{i}(\omega t - k_x x)]$. The flexural rigidity is given by $Eh^3/12(1 - \nu^2)$, where E is Young's modulus of the plate material, ν is the Poisson ratio and h is the plate thickness. Astley [13] has described a variational approach to the analysis of low frequency sound propagation in a duct with a partially flexible wall, a bulk-reacting acoustic lining and a mean fluid flow, which may be adapted to the present case by discounting the presence of the lining and putting the mean flow Mach number equal to zero. The variational

functional of Astley may then be written

$$\Phi = \rho\omega^2 \int_C \{(g/2)[(\mathrm{d}^2U/\mathrm{d}s^2)^2 + 2k_x^2(\mathrm{d}U/\mathrm{d}s)^2 + (k_x^4 - k_p^4)U^2] - UP_p\}\mathrm{d}s + \frac{1}{2}\iint_R [\nabla_t P \cdot \nabla_t P - (k^2 - k_x^2)P^2]\,\mathrm{d}R, \tag{3}$$

where ρ is the density of the gas within the duct. The Euler equations of this functional are: Eq. (2a,b), (with the constraint of zero displacement at the edges of the flexible wall), the rigid-wall boundary condition on the rigid part of the duct wall, and equality of the normal plate displacement and the normal acoustic particle displacement in the internal sound field on C (provided that the normal gradient of sound pressure is allowed to vary freely at the outer surface of the flexible wall). In the case of low frequency sound propagation in the duct, the sound pressure may be assumed approximately uniform on $\mathbf{y}$ (see the comment by Cummings [10]: "Comparisons between Cabelli's predicted coupled modal axial wavenumber data (for a non-uniform internal sound field) and those based on a plane-mode approximation show very close agreement between the two up to the cut-on frequency of the first acoustic higher order mode in the equivalent rigid-walled duct…"). If it is also assumed that the flexible duct wall has edges that are rigidly clamped and that the acoustic radiation load on the outer surface of the plate is negligible, a simple two-degrees-of-freedom Rayleigh–Ritz formulation may be implemented by taking a constant-amplitude trial function for the sound pressure,

$$P(\mathbf{y}) = P_p(s) = P_0 \tag{4a}$$

and a simple trial function for the plate displacement,

$$U(s) = U_0 \sin^2(\pi s/S). \tag{4b}$$

Eq. (4b) is (as numerical studies reveal) a reasonable approximation to the computed plate displacement at frequencies below the frequency of the second (symmetrical) transverse structural resonance of the duct walls. Insertion of Eqs. (4a) and (4b) into Eq. (3) and integration (which is straightforward) yields

$$\Phi = \rho\omega^2(g/2)U_0^2[2S(\pi/S)^4 + Sk_x^2(\pi/S)^2 + (3/8)S(k_x^4 - k_p^4)] - \rho\omega^2 P_0 U_0 S/2 - (k^2 - k_x^2)P_0^2 R/2. \tag{5}$$

Stationary values of the functional Φ are now sought, satisfying $\delta\Phi = 0$, or equivalently $\partial\Phi/\partial P_0 = 0, \partial\Phi/\partial U_0 = 0$. This leads to a system of two homogenous linear equations in P_0 and U_0, which yield the cubic dispersion relationship

$$K^3 + [(8/3)(\pi/S)^2 - k^2]K^2 + [(16/3)(\pi/S)^4 - (8/3)k^2(\pi/S)^2 - k_p^4]K + [k^2k_p^4 - (16/3)k^2(\pi/S)^4 - (2/3)\rho\omega^2 S/gR] = 0, \tag{6}$$

where $K = k_x^2$ and R represents the cross-sectional area of the duct. This equation should be approximately valid at frequencies where the sound pressure distribution within the duct is approximately plane and where the wall displacement profile may be approximated by the $\sin^2()$ relationship of Eq. (4b), i.e., below the frequency of the second (symmetrical) transverse resonance in the flexible wall. Clearly, propagating coupled modes—with real values of k_x—correspond to positive values of K, since $k_x = \pm\sqrt{K}$. Up to three propagating modes in each

direction are in principle accommodated by Eq. (6). The above formulation may easily be modified to suit the case of a square section duct with four flexible walls (and therefore no rigid walls), and then the only change required in Eq. (6) is that R is replaced by $R/4$.

2.2. A more accurate dispersion relationship

Better accuracy may be obtained, at the expense of greater complexity in the solution, by again assuming that the acoustic wave in the duct is plane, but this time finding an exact solution for the wall displacement pattern. Either the method described by Astley [13] or that of Cummings [4] may be followed (both lead to the same result), and a dispersion relationship

$$k_x = k\sqrt{1 - \mathrm{i}S\langle\beta(k_x)\rangle/kR} \tag{7}$$

is obtained in the present case, where $\langle\beta(k_x)\rangle$ is the dimensionless admittance presented by the flexible wall to the internal sound field (normalized against ρc), averaged over S. If it is again assumed that the radiation load on the outer surface of the flexible wall may be neglected then, for clamped boundary conditions along both edges of the flexible wall, an exact solution of Eq. (2a,b) may be obtained, yielding an expression for the average wall admittance,

$$\langle\beta(k_x)\rangle = \mathrm{i}\omega\rho c\left\{\frac{A_1}{\alpha_1 S}\sin(\alpha_1 S) - \frac{A_2}{\alpha_1 S}[\cos(\alpha_1 S) - 1] + \frac{A_3}{\alpha_2 S}\sinh(\alpha_2 S) + \frac{A_4}{\alpha_2 S}[\cosh(\alpha_2 S) - 1] + \frac{1}{g(k_x^4 - k_p^4)}\right\}, \tag{8}$$

where

$$\alpha_1 = \sqrt{k_p^2 - k_x^2}, \quad \alpha_2 = \sqrt{k_p^2 + k_x^2} \tag{9a, b}$$

and

$$\begin{aligned}
A_1 &= \{\alpha_1[1 + \cos(\alpha_1 S) - \cosh(\alpha_2 S) - \cos(\alpha_1 S)\cosh(\alpha_2 S)] \\
&\quad + \alpha_2\sin(\alpha_1 S)\sinh(\alpha_2 S)\}/g(k_x^4 - k_p^4)[2\alpha_1\cos(\alpha_1 S)\cosh(\alpha_2 S) \\
&\quad - 2\alpha_1 + (\alpha_1^2/\alpha_2 - \alpha_2)\sin(\alpha_1 S)\sinh(\alpha_2 S)], \\
A_2 &= \{\alpha_1\sin(\alpha_1 S)[1 - \cosh(\alpha_2 S)] \\
&\quad + \alpha_2\sinh(\alpha_2 S)[1 - \cos(\alpha_1 S)]\}/g(k_x^4 - k_p^4)[2\alpha_1\cos(\alpha_1 S)\cosh(\alpha_2 S) \\
&\quad - 2\alpha_1 + (\alpha_1^2/\alpha_2 - \alpha_2)\sin(\alpha_1 S)\sinh(\alpha_2 S)], \\
A_3 &= -A_1 - 1/g(k_x^4 - k_p^4), \\
A_4 &= -A_2\alpha_1/\alpha_2.
\end{aligned} \tag{10a–d}$$

Eq. (8) is inserted in Eq. (7), and roots of this equation are sought. The usual root-finding methods will not normally identify all the solutions of (7), because of the rather difficult, multi-branched, nature of the function on the left hand side (see the discussion by Cummings in Ref. [6]). The most reliable method of root finding is the very simplest graphical method of identifying the zero-crossings that can be seen to correspond to roots of the function, and this was employed here. It is of interest to compare results from Eqs. (6) and (7).

2.3. Numerical results of modal phase speed and comparison between the two solutions

The system parameters for the experimental duct, as used in the computations, were as follows: $E = 7.2 \times 10^{10}$ Pa, $m = 1.62$ kg/m^2, $v = 0.34$, $\rho = 1.2$ kg/m^3, $c = 344$ m/s, $h = 0.6$ mm, $S = 107$ mm, $R = 0.009$ m^2. A comparison between the phase speeds of the propagating modes, predicted from Eqs. (6) and (7), is shown in Fig. 3. The frequency range is 100–1500 Hz, and covers the range of interest in the experiments. Below 330 Hz, only one mode (“mode 1”) propagates (i.e., there is only one positive real root of Eqs. (6) and (7)), but above this frequency—which corresponds to the first transverse resonance frequency of the flexible wall, subjected to the internal acoustic load—a further mode (“mode 2”) appears, and both modes 1 and 2 propagate. At low frequencies, mode 1 travels at a speed rather less than the acoustic speed (because of the stiffness-controlled impedance of the flexible duct wall) and is an “acoustic” type mode since the power flow is predominantly in the fluid (see for example the discussion by Cummings [10]). However, around “cut-on” for mode 2, the phase speed of mode 1 falls rapidly and above 500 Hz is close to the free wave speed of a purely structural mode with one displacement maximum in the centre of the flexible wall. Mode 1 is a predominantly “structural” type mode in this frequency range, since most of the power flow is in the flexible wall. In contrast, mode 2 is essentially an “acoustic” type mode between 500 and 1500 Hz, in which range its phase speed is rather higher than the sound speed. At a frequency above the range of the plot in Fig. 3, a third mode (initially of the acoustic type) will appear, and above its cut-on frequency, both modes 1 and 2 will be of the

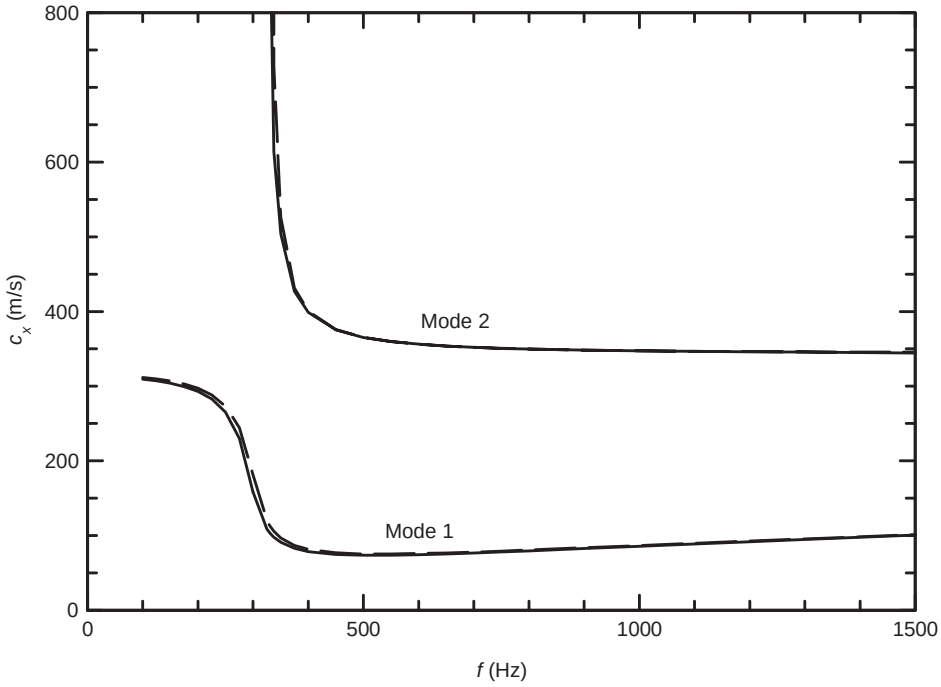

Fig. 3. Predicted phase speed of coupled modes in the experimental duct. ——, exact solution for plate motion; – – –, variational solution.

structural type. This pattern is repeated as further modes begin to propagate at successively higher frequencies.

It is observed from the data in Fig. 3 that the variational solution of Section 2.1 is overall in very close agreement with the more accurate prediction of Section 2.2. Some small discrepancies are evident around the cut-on frequency of mode 2, but these are rather insignificant. Either method would be acceptable for the prediction of the modal phase speeds in this investigation, but Eq. (7) was chosen because of its marginally greater accuracy.

3. Visualization of individual coupled modes by active control

Active control is a technique for attenuating acoustic or vibratory fields which involves the addition, to the "primary" acoustic or structural wave, of a "secondary" wave of the same form but with opposite sign. These two waves cancel each other to leave a null acoustic field. The implementation of this rather simple idea usually requires the real-time adaptation of convolution coefficients in a filter, the output of which is the driving signal of the secondary source or—very rarely—a full prediction of the filter coefficients based on *complete* knowledge of propagation and transducers, i.e., on comprehensive modelling of the configuration considered. The present method of control is based on a generalization of active control of plane guided waves, and here the experimental identification of wave characteristics plays the role of modelling. In the broader context discussed in Section 1, a further development of the ideas presented in this paper would benefit from auto-adaptive control, which would however require partial modelling in the present case.

3.1. Generalization of the active control of plane guided sound waves

As mentioned in the Introduction, active control is applied here to *structural* waves in the flexible wall (for reasons which will later become apparent). However, the secondary source is *acoustic*, and the vibrational cancellation signal results from the structural response to fluid wave motion induced by this source.

If the structural/acoustic configuration considered in this paper gives rise to just one dispersive coupled mode made up of an acoustic plane wave and a transverse structural mode, say $\Psi(s)$, the primary vibratory acceleration at (x,s) may be expressed by $\gamma_0(x,s)=\mu_0(x)\Psi(s)$ and the acceleration response at (x,s) arising from an acoustic source at x_s can be written $G(x,x_s,s)=v(x,x_s)\Psi(s)$. Control of the acceleration in the least-mean square sense follows the well-known minimization algorithm, written

$$\min_{\phi} F(\phi)=\min_{\phi}\left\| G(x,x_s,s)\phi+\gamma_0(x,s)\right\|^2_{L^2(\Gamma)}, \tag{11}$$

where ϕ is the driving signal of the secondary acoustic source at x_s, also termed the "secondary control", $G(x,x_s,s)\phi$ constitutes the secondary vibratory field, and Γ is the part of the yielding wall such that $x\geqslant x_0$ and $x\geqslant x_s$ if x_0 is the primary source location. The L^2-norm in a domain Ω is defined in a continuous form as $\|f(u)\|^2_{L^2(\Omega)}=\int_\Omega |f(u)|^2\,\mathrm{d}u$. In the case where $\mathbf{f}$ is a column vector, $|\mathbf{f}|^2=\mathbf{f}^*\cdot\mathbf{f}$, the asterisk denoting the transpose conjugate (or conjugate in the case of a scalar). The optimal control ϕ^{opt} that minimizes $F(\phi)$, a quadratic function of ϕ, is obtained by annulling the

variation of F resulting from a variation of ϕ .This results in

$$\phi^{opt} = -\frac{1}{||G||^2_{L^2}} \int_{\Gamma} G^*(x, x_s, s)\gamma_0(x, s)\,\mathrm{d}x\,\mathrm{d}s, \tag{12}$$

leading to $F(\phi^{opt}) = F_{min} = 0$. The least-mean square norm is the modulus if the domain is made up of only one point (x, s), where the accelerometer is located, and the solution ϕ (for only one point with $x \geqslant x_0$ and $x \geqslant x_s$) has the same value as that obtained from (12), thus resulting in null acceleration at (x, s) with the very interesting consequence that the vibratory field is also zero everywhere beyond point $x \geqslant (x_0, x_s)$. The acoustic pressure would also be zero on the far side of this point.

Consider now two coupled modes propagating simultaneously. The acceleration at any point has four components, associated with the positive and negative travelling waves for each mode (these are numbered 1 and 2, respectively, for the slow and fast waves; see Fig. 3). For the sake of generality we introduce the transverse structural modal shape of each of them, say $\psi_1(s)$ and $\psi_2(s)$. The acceleration along the wall is therefore written

$$\gamma_0(x, s) = \underbrace{(a_{01}\mathrm{e}^{-\mathrm{i}k_1 x} + b_{01}\mathrm{e}^{\mathrm{i}k_1 x})\Psi_1(s)}_{\gamma_{01}(x,s)-\text{slow}} + \underbrace{(a_{02}\mathrm{e}^{-\mathrm{i}k_2 x} + b_{02}\mathrm{e}^{\mathrm{i}k_2 x})\Psi_2(s)}_{\gamma_{02}(x,s)-\text{fast}} \tag{13}$$

or, insofar as each component $\gamma_{01}(x, s)$ and $\gamma_{02}(x, s)$ can be seen as independent, γ_0 can be written in matrix form:

$$\boldsymbol{\gamma}_0(x, s) = \begin{Bmatrix} \gamma_{01}(x, s) \\ \gamma_{02}(x, s) \end{Bmatrix} = \begin{bmatrix} \Psi_1(s) & 0 \\ 0 & \Psi_2(s) \end{bmatrix} \left(\begin{bmatrix} \mathrm{e}^{-\mathrm{i}k_1 x} & 0 \\ 0 & \mathrm{e}^{-\mathrm{i}k_2 x} \end{bmatrix} \begin{Bmatrix} a_{01} \\ a_{02} \end{Bmatrix} + \begin{bmatrix} \mathrm{e}^{\mathrm{i}k_1 x} & 0 \\ 0 & \mathrm{e}^{\mathrm{i}k_2 x} \end{bmatrix} \begin{Bmatrix} b_{01} \\ b_{02} \end{Bmatrix} \right)$$

or

$$\boldsymbol{\gamma}_0(x, s) = \boldsymbol{\Psi}(\mathbf{E}_- \mathbf{a}_0 + \mathbf{E}_+ \mathbf{b}_0). \tag{14}$$

Assuming a linear and passive termination, the vectors $\mathbf{a}_0$ and $\mathbf{b}_0$ can be related via a reflection matrix $\mathbf{R}$, which implies

$$\boldsymbol{\gamma}_0(x, s) = \boldsymbol{\Psi}(\mathbf{E}_- + \mathbf{E}_+ \mathbf{R})\mathbf{a}_0. \tag{15}$$

Matrix $\mathbf{R}$ is diagonal if mode $\Psi_1(s)$ (or $\Psi_2(s)$) generates only mode $\Psi_1(s)$ (or $\Psi_2(s)$) upon reflection at the termination. In the same way, the structural response from an acoustic source located at x_s, radiating two coupled modes, may be written

$$\mathbf{G}(x, x_s, s) = \boldsymbol{\Psi}(\mathbf{E}_- + \mathbf{E}_+ \mathbf{R})\mathbf{a}_s. \tag{16}$$

Given $\Psi_1(s)$, $\Psi_2(s)$ and, in particular, $\Psi_1(s) = \Psi_2(s) \equiv \Psi(s)$ (the first structural mode such that $|\Psi(0)| = 1$, where $s = 0$ defines the centreline of the vibrating wall), at first sight an array of four transducers would seem to enable measurement of the four amplitudes $(\mathbf{a}_0, \mathbf{b}_0)$ or $(\mathbf{a}_s, \mathbf{b}_s)$ to be made, provided phase speeds c_1 and c_2 are known.

With only one secondary source the driving signal is a (complex) scalar, but the response is a vector with two components, $G_1(x, x_s, s)$ and $G_2(x, x_s, s)$, representing the emission of each structural wave (slow and fast) by the secondary source. Here, minimization at one point in the least-mean square sense results in a reduction but not complete cancellation. The attenuation obtained is totally determined by the control system configuration and cannot be altered. On the

other hand, it could be possible to cancel one of the two waves and to detect the other, transmitted beyond the control accelerometer (and for $x \geqslant (x_0, x_s)$). This approach would make it possible not only to visualize each coupled mode in isolation, but also to intercept the "structural mode" (i.e., the slow wave, with most of its power flow in the structural motion) that can be responsible for the flanking effect in silencers, mentioned in Section 1. With two secondary sources, and provided certain hypotheses concerning the linear independence in their responses were satisfied, it could be possible to cancel out both fast and slow waves, i.e., the entire acceleration. Such an approach would, of course, no longer be regarded as being a way of visualizing each of the coupled modes separately.

If one focuses on the cancellation of one wave by one secondary source, the choice of the type of control must be made. Usually, the algorithm of Eq. (11) is associated with auto-adaptive control. Its implementation requires adaptation of the coefficients in a digital signal processor. In the configuration dealt with here control in delayed time, with a totally predetermined controller, leads to the same outcome. The advantage of this method is that the implementation of only the physical experiment is needed. The drawback is that a relatively complete model is required. This can be either numerical, or experimental in the sense that the necessary characteristics are identified from measurements. In this exploratory work, full numerical modelling was not justified and therefore experimental modelling was chosen. The identification was carried out with the use of a genetic algorithm.

3.2. Measurements and identification of wave characteristics

Measurements were carried out on the duct shown in Fig. 4. The two loudspeakers played the roles of the primary and secondary acoustic sources. The loudspeaker located at one end of the

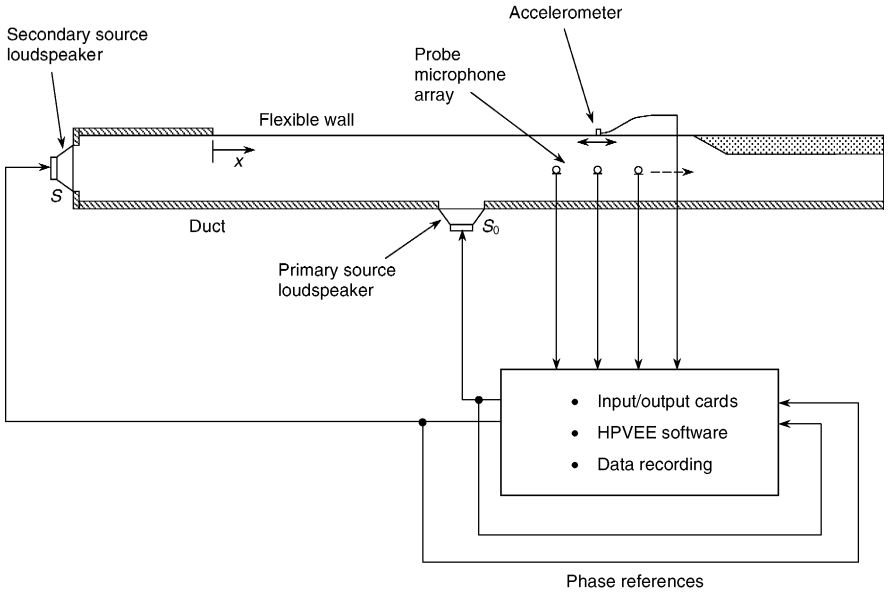

Fig. 4. Experimental arrangement of the duct.

duct acted as the secondary source, and the other (approximately half-way along the duct in one of the rigid walls, as shown in Fig. 4) provided the primary wave field. The sound pressure inside the duct was detected by 16 small microphones placed at 20 mm intervals along the duct axis, in one of the rigid walls adjacent to the flexible wall. With 16 input channels in the recording system, 50 measurement points were employed, and these required four separate recordings, each taken with a phase reference signal. Only one accelerometer (0.65 g B&K) was used to detect the wall acceleration and with 50 measurement points on the centreline of the flexible wall, this required 50 separate recordings. HPVEE graphic software, installed on a PC, was used to conduct the test procedure. The distance along the flexible wall, from the rigid termination, is denoted x (see Fig. 4).

In Figs. 5(a)–(d) and 6(a)–(d) are shown, respectively, vibratory acceleration and acoustic pressure (amplitude and phase) at both 600 and 800 Hz with source S operating, at 50 points from $x = 20$ mm to 1.0 m by steps of 20 mm. The wall acceleration shows strong undulations in both amplitude and phase at both measurement frequencies. This suggests the existence of a standing wave system comprising two positive-travelling coupled structural/acoustic modes (having

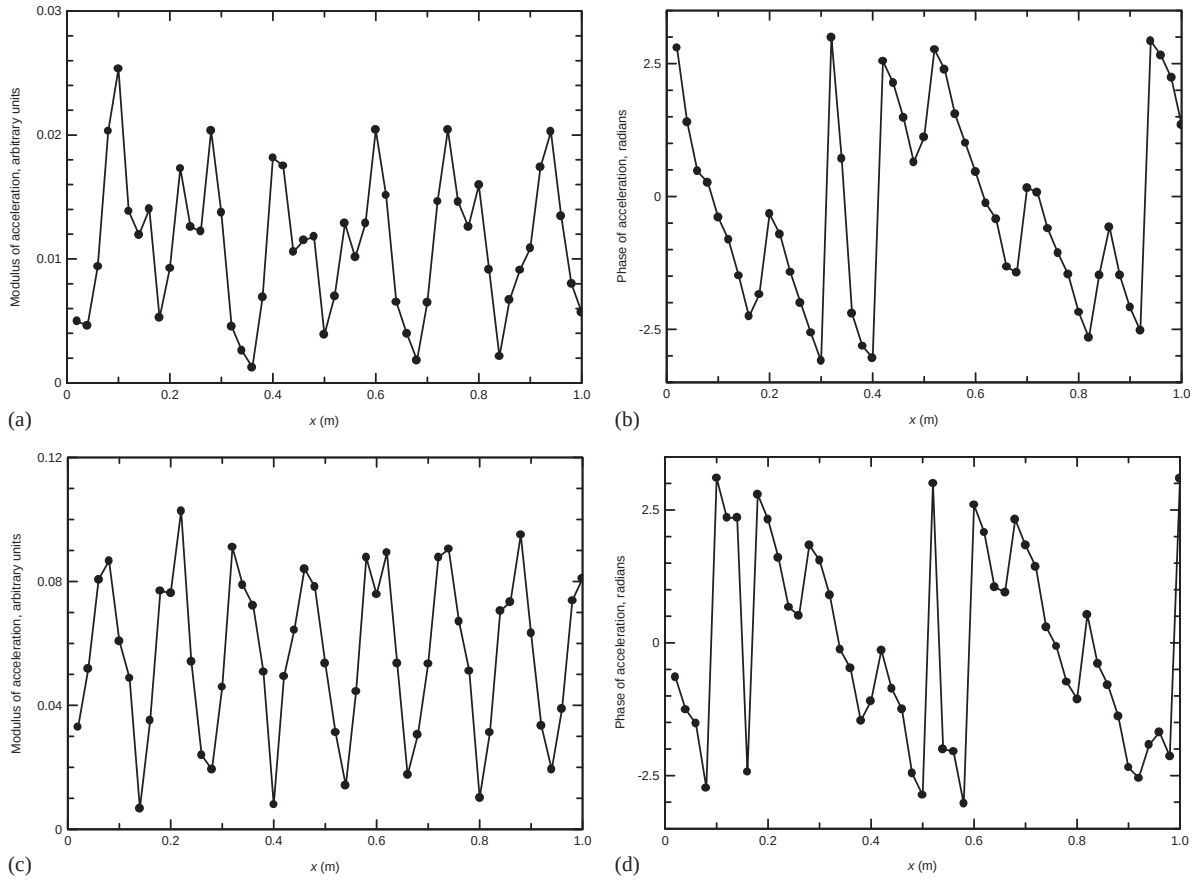

Fig. 5. Acceleration on the flexible wall with source S operating. (a) Modulus, 600 Hz; (b) phase, 600 Hz; (c) modulus, 800 Hz; (d) phase, 800 Hz.

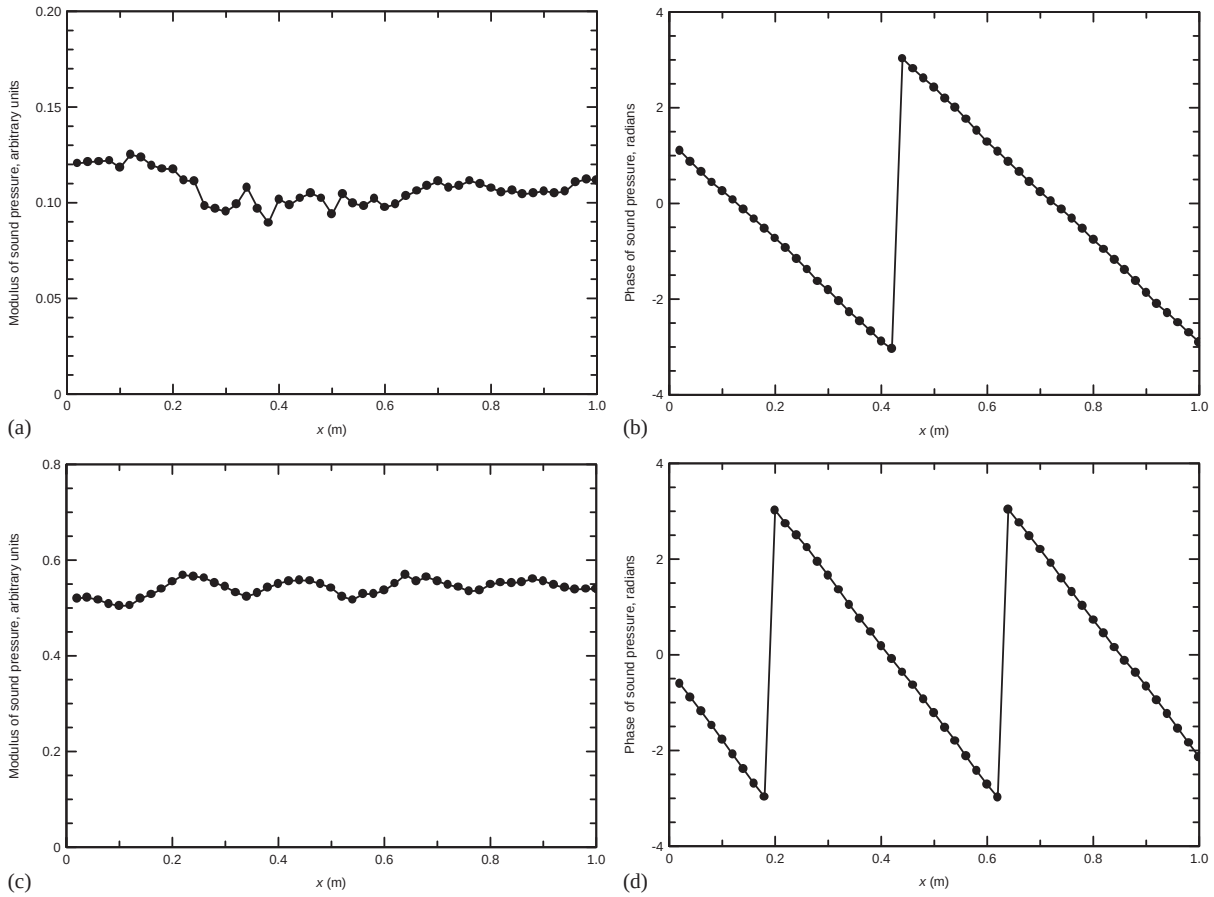

Fig. 6. Sound pressure distribution the duct with source S operating. (a) Modulus, 600 Hz; (b) phase, 600 Hz; (c) modulus, 800 Hz; (d) phase, 800 Hz.

differing phase speeds; see Fig. 3) and two reflected coupled modes at both 600 Hz and 800 Hz, given that the termination was unlikely to be completely anechoic for either mode. The acoustic pressure pattern, on the other hand, much more closely resembles a progressive wave since it has an almost constant amplitude and a linear phase variation with x. The phase slope is consistent with phase speeds of approximately 360 m/s ($k = 10.5$ rad/m) and 350 m/s ($k = 14.4$ rad/m) at 600 and 800 Hz respectively. It would seem, from these values, that the fast coupled mode dominates the sound field. This is consistent with the results of Astley, Cummings and Sormaz [7], who show that—albeit in an acoustically lined duct with one flexible wall—the "structural", slow, mode makes little contribution to the sound field, even though it can be a large contributor to the wall vibration pattern. One can assume that this behaviour applies also in the case of unlined ducts.

From the results of Section 2, it is clear that—at each of the frequencies of interest here—two coupled modes can propagate. At each point in the duct, both the acceleration and sound pressure have the form of Eq. (13). If measurements are carried out at I points, located at distances x_i,

these data may be written in a column vector $\mathbf{m}$ made up of I elements which, according to the model, has the form

$$\mathbf{m} = \begin{bmatrix} e^{-ik_1x_1} & e^{ik_1x_1} & e^{-ik_2x_1} & e^{ik_2x_1} \\ e^{-ik_1x_2} & \cdots & \cdots & \cdots \\ \cdots & \cdots & \cdots & e^{-ik_2x_{I-1}} \\ e^{-ik_1x_I} & e^{ik_1x_I} & e^{-ik_2x_I} & e^{ik_2x_I} \end{bmatrix} \begin{Bmatrix} a_1 \\ b_1 \\ a_2 \\ b_2 \end{Bmatrix} = \mathbf{Ea}, \tag{17}$$

where $\mathbf{E}$ is an $(I,4)$ matrix. Where the wavenumbers are given at each frequency (e.g., from the models described in Section 2), the least-mean square solution is $\mathbf{a} = (\mathbf{E}^*\mathbf{E})^{-1}\mathbf{E}^*\mathbf{m}$. Of course, there are inevitable predictive inaccuracies associated with the wavenumbers, however small. It may be shown that, if fixed values of the wavenumbers are taken in this way, the errors result in a dependence of the elements of the vector $\mathbf{a}$ (the complex wave amplitudes) on the number of points I considered. Consequently, the decision has been taken to identify the wavenumbers k_1 and k_2 as well as the wave amplitudes. The problem now consists of minimizing $|\mathbf{Ea} - \mathbf{m}|^2$ by adjusting a_1, b_1, a_2 and b_2, together with k_1 and k_2. The solution is sought by the use of a genetic algorithm, which turned out to be suitable for this particular application. It was used in preference to more ''standard'' techniques such as the generalized Newton–Raphson method because of its generality and relative robustness. (The book by Goldberg [14] gives a good introduction to the applications of genetic algorithms and includes a discussion on robustness.) The genetic algorithm employed here follows the pattern below:

(a) Vector-individuals $\mathbf{d} \in \mathbb{C}$ in the sense that each of the six components $d_i \in \mathbb{C}$. Only the real parts of the wavenumbers will be retained. A first population of M (≈ 40) individuals is built by randomly choosing their components. The plots in Fig. 3 provide suitable initial values for the wavenumbers.

(b) For the members of the population, the values of

$$f(\mathbf{d}) = |\mathbf{E}(k_1, k_2)\mathbf{a} - \mathbf{m}|^2 \tag{18}$$

are calculated and the individuals $\mathbf{d}$ are classified in the order of increasing value of $f(\mathbf{d})$. The first individual is therefore the ''best fitted''.

(c) The selection of the parents in the population results from a procedure akin to that known as the ''roulette method'', i.e., the greatest chance to become parents occurs for individuals at the top of the list organized above.

(d) Components of individuals which play the roles of parents are crossed and/or mutated. One should remember that individuals are made up of numerical values. The set of ''offspring'' constitutes the next generation. At each generation the number of individuals is of the same order of magnitude.

(e) Again, for each member of the new generation, $f(\mathbf{d})$ is calculated and the individuals $\mathbf{d}$ are again classified in the order of increasing value of $f(\mathbf{d})$. If necessary, one should return to step (c).

(f) The procedure is halted when the minimum value of $f(\mathbf{d})$ no longer decreases or is sufficiently low. Then the values of the coefficients corresponding to $f^{\min}$, i.e., the minimum value of $f(\mathbf{d})$, are deduced.

Table 1 gives the values of the parameters obtained at 600 and 800 Hz when either source S or source S_0 is switched on (amplitudes are on an arbitrary scale and phases are in radians). These values stem from measurements carried out beyond the two sources in the x direction, i.e., between $x = 0.7$ and 1.0 m. (The sequences of measurements here were separate from those

Table 1
Wavenumbers and modal coefficients with the two sources operating separately

Frequency (Hz)	k_1 (m^{-1}) (slow wave)	k_2 (m^{-1}) (fast wave)	a_1 (m/s^2)	b_1 (m/s^2)	a_2 (m/s^2)	b_2 (m/s^2)
Source S_0 operating						
600	49.2	10.2	$0.226e^{i1.392}$	$0.072e^{i0.0}$	$0.338e^{-i2.926}$	$0.021e^{i1.328}$
800	62.1	14.6	$0.021e^{i2.060}$	$0.004e^{i0.173}$	$0.262e^{-i1.213}$	$0.021e^{-i2.085}$
Source S operating						
600	49.2	10.2	$0.267e^{-i1.459}$	$0.072e^{-i2.662}$	$0.352e^{i0.268}$	$0.027e^{-i1.935}$
800	62.1	14.6	$0.185e^{i2.845}$	$0.072e^{i1.737}$	$0.276e^{-i0.968}$	$0.013e^{-i2.293}$

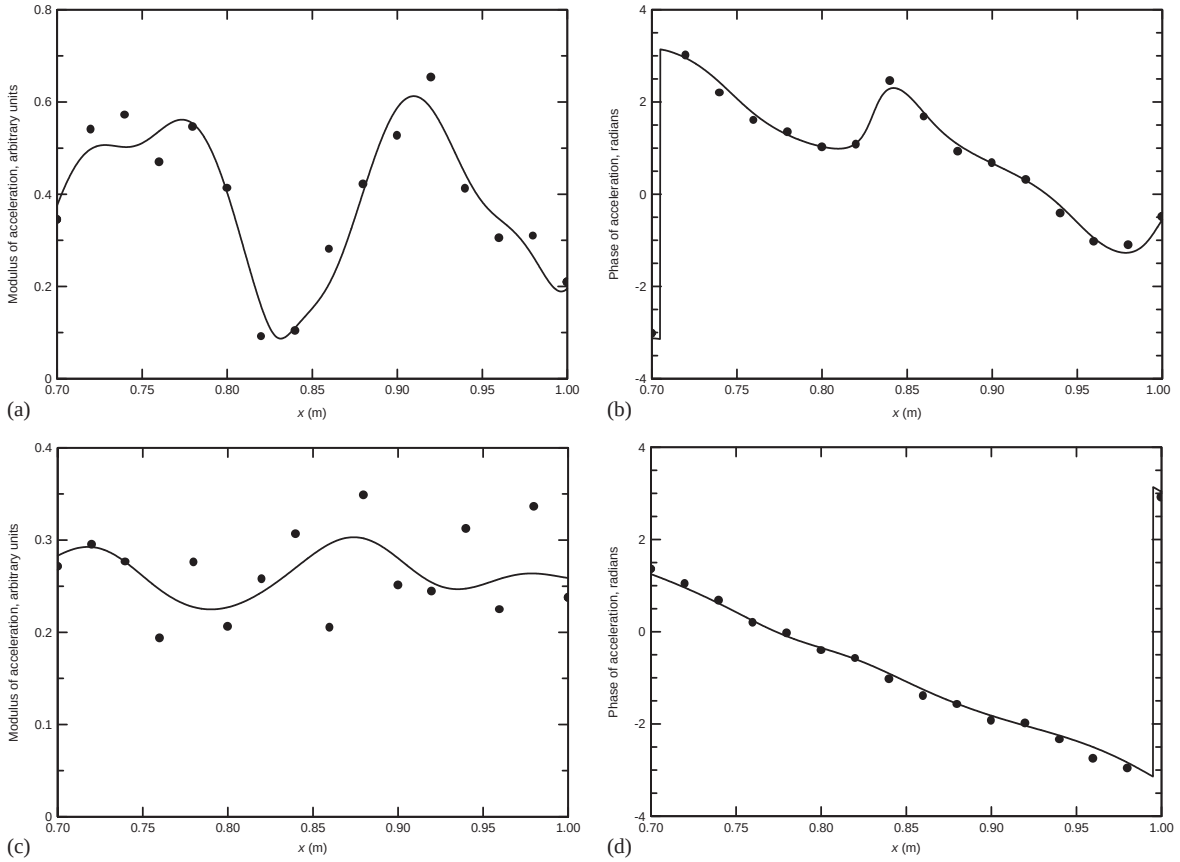

Fig. 7. Reconstruction and measured data of the acceleration on the flexible wall with source S_0 operating. (a) Modulus, 600 Hz; (b) phase, 600 Hz; (c) modulus, 800 Hz; (d) phase, 800 Hz. ——, reconstruction; •, measured data.

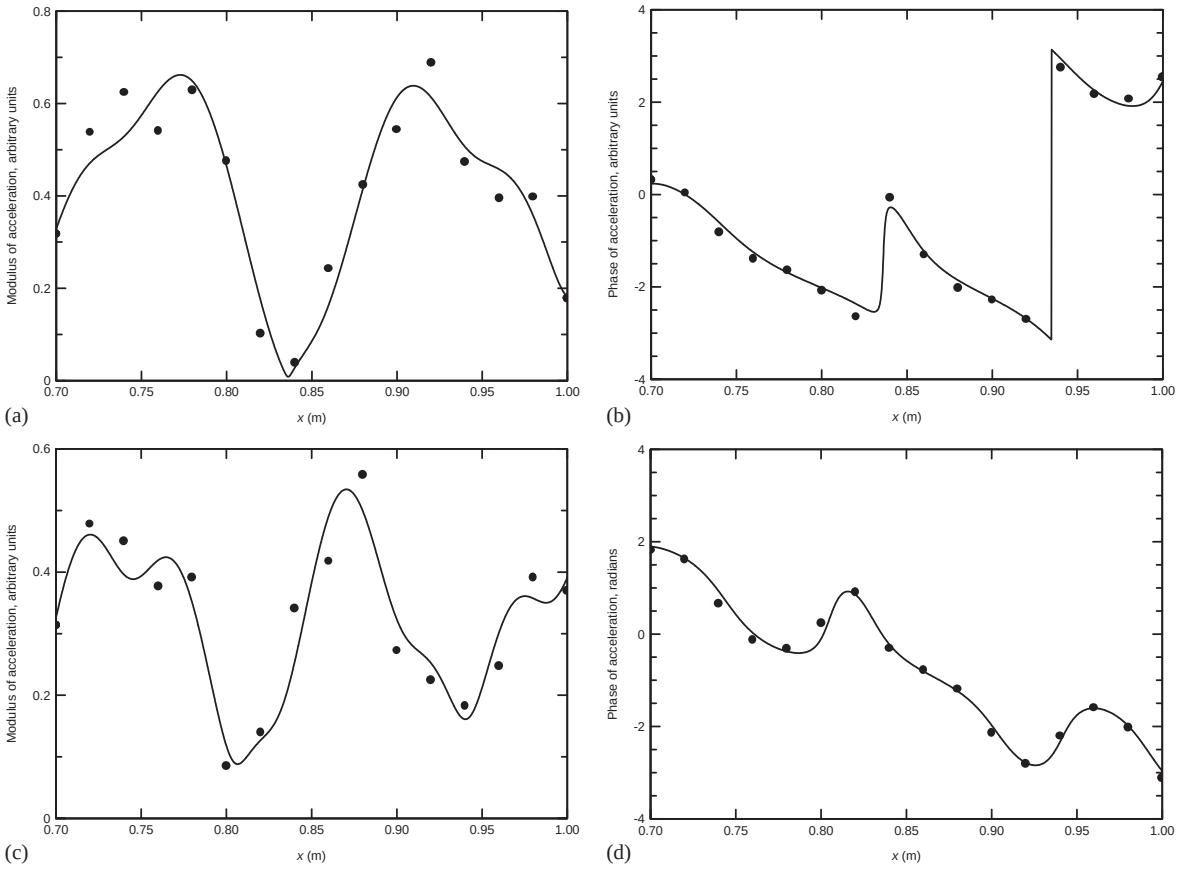

Fig. 8. Reconstruction and measured data of the acceleration on the flexible wall with source S operating. (a) Modulus, 600 Hz; (b) phase, 600 Hz; (c) modulus, 800 Hz; (d) phase, 800 Hz. ——, reconstruction; •, measured data.

leading to Figs. 5 and 6.) Figs. 7 and 8 show the "reconstruction", via the use of Eq. (13), of the vibratory acceleration amplitude and phase from the numerical values obtained from the identification procedure, together with the measured data. Comparison between the data in Figs. 5 and 8 reveals a satisfactory reproducibility in the relative values of amplitude and in the phase, between independently measured sets of data. Concerning the reconstruction of the measured data, in Figs. 7 and 8, one may note that the phases are always in good agreement with the measurements, though the agreement is less good in the case of the amplitudes. This might suggest that the model with just two propagating waves is insufficient and that, perhaps, evanescent waves ought also to be included in the model.

In Table 2 a comparison is made, between the wavenumbers of the fast and slow waves at 600 and 800 Hz obtained from the genetic algorithm, and those predicted from Eqs. (7) to (10). The latter figures were computed with $c = 344$ m/s. The agreement between the "identified" and computed values is close in all cases, and certainly confirms the experimentally observed fast and slow waves as being two types of coupled mode.

Table 2
Comparison between fast and slow modal wavenumbers, predicted and inferred from the genetic algorithm

Frequency (Hz)	k_1 (slow wave) (m^{-1}), Eq. (7)–(10)	k_1 (slow wave) (m^{-1}), genetic algorithm	k_2 (fast wave) (m^{-1}), Eq. (7)–(10)	k_2 (fast wave) (m^{-1}), genetic algorithm
600	50.6	49.2	10.6	10.2
800	63.2	62.1	14.4	14.6

3.3. Visualization of individual coupled modes by active control

Active attenuation is employed here for cancellation of the slow wave, thus leaving the fast wave propagating alone, and vice versa, with the wider context mentioned in Section 1 still being borne in mind. Considerations of flanking mechanisms in silencers would perhaps give priority to cancellation of the structural mode, i.e., the slow wave, in the frequency range studied. It will be assumed that the initial problem in hand concerns the cancellation of *structural* motion in the flexible wall by a purely *acoustic* secondary source.

Two coupled propagating modes in both the positive and negative x directions will be taken into account, to allow for structural and acoustic reflections from the duct termination. According to Eqs. (15) and (16), the total acceleration arising from both primary and secondary sources is

$$\boldsymbol{\gamma}(x,s) = \boldsymbol{\Psi}(\mathbf{E}_- + \mathbf{E}_+\mathbf{R})(\mathbf{a}_s\phi + \mathbf{a}_0) = \mathbf{G}(x,x_s,s)\phi + \boldsymbol{\gamma}_0(x,s). \tag{19}$$

Table 1 enables $\mathbf{G}$ to be found when the voltage applied to source S is recorded. Algorithm (11) applied to $\boldsymbol{\gamma}(x,s)$ leads to $\phi_{opt} = -(1/\|\mathbf{G}\|^2_{L^2}) \int_\Gamma \mathbf{G}^*(x,x_s,s)\boldsymbol{\gamma}_0(x,s)\,\mathrm{d}x\,\mathrm{d}s$, i.e., Eq. (12) extended to vectors, and results in (the L^2-norm on Γ being tacit)

$$F(\phi_{opt}) = F_{\min} = -\frac{1}{\|\mathbf{G}\|^2}\left|\int_\Gamma \mathbf{G}^*\boldsymbol{\gamma}_0\,\mathrm{d}x\,\mathrm{d}s\right|^2 + \|\boldsymbol{\gamma}_0\|^2. \tag{20}$$

As long as $\mathbf{G}$ and $\boldsymbol{\gamma}_0$ are not collinear vectors, the relation $0 \leqslant \left|\int_\Gamma \mathbf{G}^*\boldsymbol{\gamma}_0\,\mathrm{d}x\,\mathrm{d}s\right|^2 < \|\mathbf{G}\|^2\|\boldsymbol{\gamma}_0\|^2$ holds and, subsequently, $0 < F_{min} \leqslant \|\boldsymbol{\gamma}_0\|^2$. Only a reduction in wave amplitude is possible, not a total cancellation. On the contrary, algorithm (11) applied to just one component of $\boldsymbol{\gamma}$, say γ_1, leads to $\phi_1^{opt} = -(1/\|G_1\|^2) \int_\Gamma G_1^*(x,x_s,s)\gamma_{01}(x,s)\,\mathrm{d}x\,\mathrm{d}s = -(a_{01}/a_{s1})$, totally cancelling γ_1 but leading to

$$\gamma_{2res}(x,s) = G_2(x,x_s,s)\phi_1 + \gamma_{02}(x,s) = \Psi(s)(\mathrm{e}^{-\mathrm{i}k_2x} + \mathrm{e}^{\mathrm{i}k_2x}R_{22})(-a_{s2}a_{01}/a_{s1} + a_{02}), \tag{21}$$

a non-zero quantity if $(a_{02}/a_{s2} - a_{01}/a_{s1}) \neq 0$, i.e., as long as $\mathbf{G}$ and $\boldsymbol{\gamma}_0$ are not collinear vectors. A similar expression for $\phi_2^{opt} (= -a_{02}/a_{s2})$, obtained for the cancellation of $\gamma_2(x,s)$, generates $\gamma_{1res}(x,s)$ having a form analogous to (21), with appropriate changes in the indices.

A necessary hypothesis for the validity of Eq. (21) is that the reflection matrix $\mathbf{R}$ has to be diagonal and identical for both the primary acceleration and the structural response. For the slow wave this implies $b_{01} = R_{11}a_{01}$ and $b_{s1} = R_{11}a_{s1}$, and similarly for the fast wave, i.e., $b_{02} = R_{22}a_{02}$ and $b_{s2} = R_{22}a_{s2}$. It so happens that this hypothesis is reasonably acceptable for the fast waves, which are absorbed well by the termination at both frequencies. For the slow waves, at 600 Hz, it is still acceptable, but is rather tenuous at 800 Hz. For the time being, however, the

hypothesis will be accepted, as it will later become evident that it does not prevent the desired result from being obtained.

The other hypothesis about the non-collinearity between primary acceleration and structural response vectors is verified as the measurements yield $\left|(a_{02}a_{s2} - a_{01}/a_{s1})\right| = 0.44$ at 600 Hz and 0.85 at 800 Hz.

Now the residual field embodied in Eq. (21) is made up of a progressive wave in e^{-ik_2x} provided $|R_{22}| \ll 1$ or $|b_{s2}| \ll |a_{s2}|$. Similarly, control $\phi_2^{opt} = -a_{02}/a_{s2}$ leaves a residual progressive wave in e^{-ik_1x} when $|R_{11}| \ll 1$ or $|b_{s1}| \ll |a_{s1}|$. According to coefficients identified from measurements at 600 Hz, one has $|b_{s1}|/|a_{s1}| \approx 0.27$ and $|b_{s2}|/|a_{s2}| \approx 0.08$. The residual fast wave ought therefore to be "more" progressive than the residual slow wave. In the experiments, knowledge of the primary and secondary fields gives optimal control. Both primary and secondary sources were activated and measurements of vibratory acceleration along the centreline of the flexible duct wall were taken. Figs. 9(a–d) show the residual fields associated with the slow and fast waves at 600 Hz. Comparison is made between the results expected from the calculations and measured data. The fast wave, remaining after cancellation of the slow wave, may be seen to be essentially a

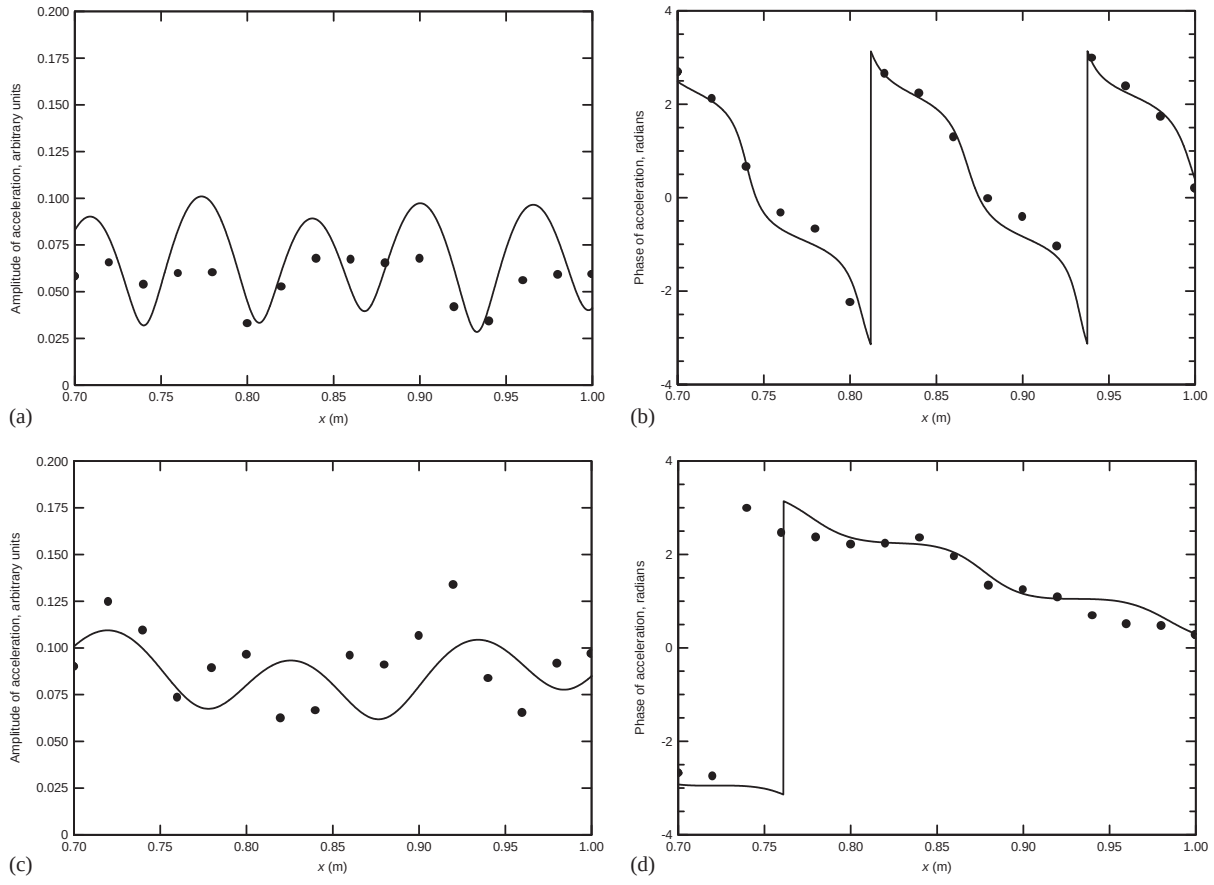

Fig. 9. Isolation of the slow and fast waves by active control, at 600 Hz. (a) Modulus of slow wave; (b) phase of slow wave; (c) modulus of fast wave; (d) phase of fast wave. ——, simulation; •, measured data.

progressive wave when one considers the almost linear variation of the phase versus distance. The phase variation, in the case of the remaining slow wave, is more perturbed by oscillations arising from reflection at the duct termination. Nevertheless, the discrimination between both waves is clear.

In Fig. 10 are shown the residual fields at 800 Hz and, with $|b_{s1}|/|a_{s1}| \approx 0.39$ and $|b_{s2}|/|a_{s2}| \approx 0.05$, the remaining slow wave is, here too, not truly progressive. However, two different slopes in the phases, at the two frequencies, are clearly apparent. Better accuracy in phase speed is obtained from the linear nature of the phase variation for the fast wave, which is consistent with a progressive wave. The same type of oscillation as before is observed in the phase variation for the residual slow wave again—it can be assumed—caused by reflection from the termination. On the other hand, the discrimination between the two waves is again quite clear. It is apparent, from Figs. 9(a)-(d) and 10(a)-(10d), that the predictions of the residual fields for both the slow and fast waves are better in terms of phase than amplitude. This may, as suggested earlier, be caused in part by the neglect of the evanescent modes, which would inevitably have been present in the experimental duct.

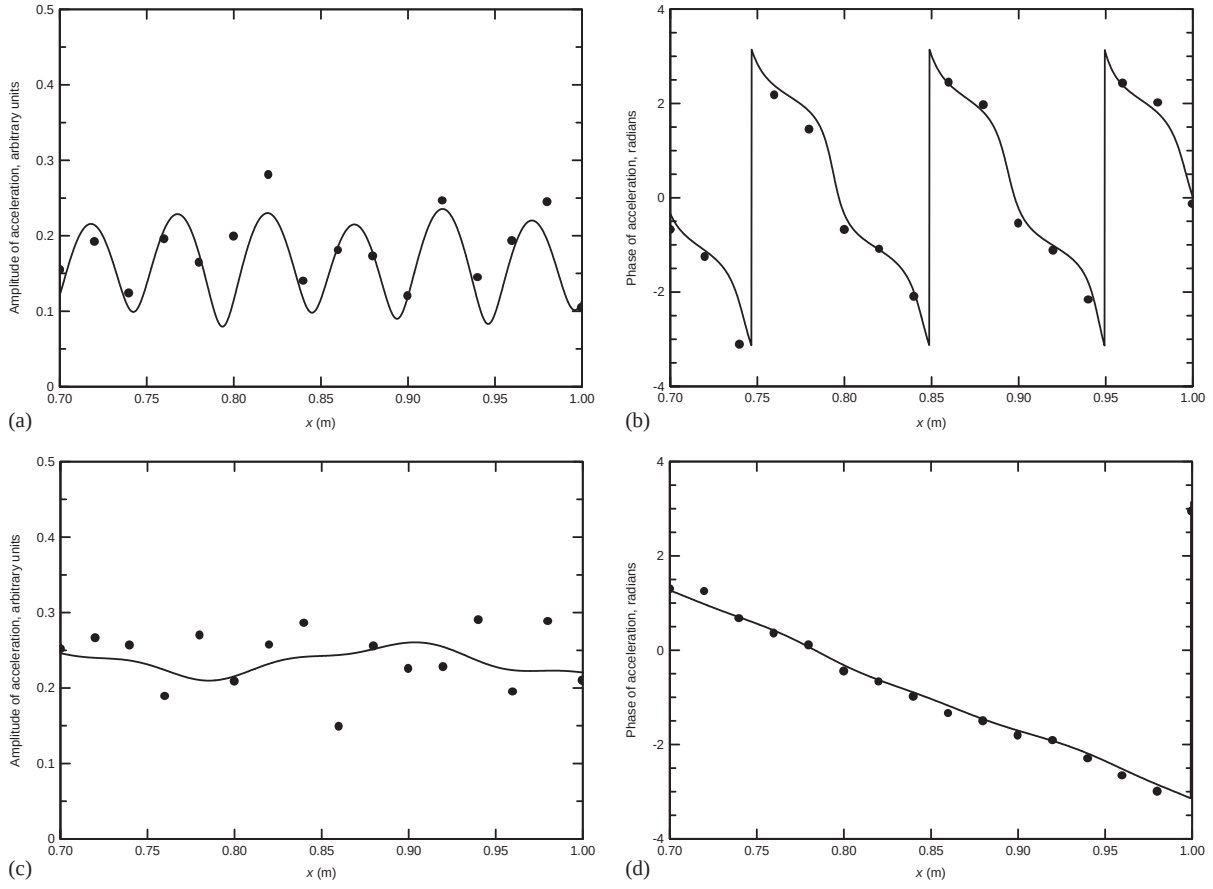

Fig. 10. Isolation of the slow and fast waves by active control, at 800 Hz. (a) Modulus of slow wave; (b) phase of slow wave; (c) modulus of fast wave; (d) phase of fast wave. ——, simulation; •, measured data.

The results presented here indicate that it is possible to visualize, separately, the slow and fast waves from the primary source in the experimental system, by the use of active control with a purely *acoustic* secondary source, based on measurements of the *structural* wave field. The data in Figs. 6(a–d) indicate that the fast acoustic wave dominates the sound field in the duct, and one may ask whether it would be possible to use active control by an acoustic secondary source, based on measurements of the *acoustic* field, to cancel this fast wave and leave only the slow coupled mode propagating. This is certainly the case. Indeed, the optimal control of the fast *acoustic* wave at 600 Hz turns out to be $\phi = 0.966\,e^{-i0.04}$ while the optimal control for the structural fast wave in the experiments reported here is $\phi = 0.959\,e^{-i0.05}$. The driving signals would therefore be effectively identical in the two cases, and the residual slow structural wave with active control of the acoustic field would be essentially that of Figs. 9(a–d). Equally, at 800 Hz, optimal control of the fast acoustic wave leads to $\phi = 1.04\,e^{i2.85}$ while, in the experiment with structural/acoustic control, one has $\phi = 0.94\,e^{i2.90}$, resulting in the essentially same residual slow wave field as that in Figs. 10(a–d). On the other hand, because of the very weak acoustic component in the slow waves, it is not possible to use active control, based on the measured *acoustic* field, to cancel the slow wave and visualize the fast wave in isolation.

4. Conclusions

In the flexible-walled duct investigated here, it was expected that two coupled structural/acoustic modes would propagate at the test frequencies. On this basis, and given that the acoustic and structural termination of the test duct was not perfectly anechoic, a genetic algorithm was employed to identify the structural parts of the two incident, and two reflected, coupled modes in terms of amplitude and phase speed. Comparisons between the measured vibration field on the flexible wall of the duct and the vibration field "reconstructed" from these amplitudes and phases revealed excellent agreement between measured and reconstructed phase, but more modest agreement between measured and reconstructed amplitude. It is not clear whether the poorer agreement in the case of the amplitude was caused by the genetic algorithm or, possibly, by the neglect of evanescent coupled modes. Since increasing the number of iterations in the algorithm failed to improve the agreement, one is tempted to question the accuracy of the two propagating mode model, in which evanescent modes are ignored.

Notwithstanding the above comments, and on the basis of the two propagating mode model, the exploratory attempts reported here, to visualize the two modes separately by eliminating one by active control in order to observe the other, were largely successful. The method of active control was implemented in delayed time. In this method the amplitude of the residual wave is modified, but not the phase speed or the phase. The simulations of the residual vibration fields—with active control—for the fast and slow waves were in good agreement with measured data in terms of phase, but rather less good agreement in terms of amplitude. This is not, perhaps, surprising in view of the relatively poor identification of amplitudes of the fast and slow wave components, in contrast to the good agreement between reconstructed and measured phases.

Although it has been possible to demonstrate a good measure of success in isolating the fast and slow waves by active control, the results presented here suggest that the physical description of the wave coupling employed in this study may be inadequate (for example, by the neglect of the

evanescent modes), and that the number of propagation parameters is insufficient. Alternatively, it is possible that non-idealities in the experimental duct apparatus, such as in the edge clamping arrangements, may have been responsible for the discrepancies between simulation and measurement. It may be that a more detailed analysis of coupled mode propagation—for example by the use of finite element analysis—would furnish a more complete and accurate physical description, particularly in terms of coupled mode reflection from discontinuities, together with better data on the propagation parameters.

A salient point is that the isolation of *structural* waves by an *acoustic* secondary source was quite likely a severe test of the active control method employed in this investigation, and that better results might have been obtained by the use of a vibrational secondary source. It was not within the scope of the project to investigate this possibility, but it should certainly be a part of any future, more comprehensive, study of the active control of coupled structural/acoustic waves in ducts.

At all events, the separate visualization of each wave type, in problems involving the coexistence of several types of wave, appears to be new field of investigation in the use of active control. It may be that active control techniques, related to that employed here, could be of use in noise control applications, for example in the active cancellation of predominantly structural type coupled modes (the ''slow'' waves described here) in duct silencers, which can (as previously mentioned) act as ''flanking'' mechanisms.

Acknowledgements

Some of the research reported in this paper was conducted by one of the authors (AC) in a visiting capacity at the Laboratoire de Mécanique de Rouen (LMR), INSA de Rouen, France, and the support of this institution, as well as the use of its facilities, is acknowledged. The authors are also grateful to the referees for suggesting improvement in the paper.

References

[1] P.M. Morse, K.U. Ingård, *Theoretical Acoustics*, McGraw-Hill, New York, 1968 (see Chapter 9).
[2] A. Cabelli, The propagation of sound in a square duct with a non-rigid side wall, *Journal of Sound and Vibration* 103 (1985) 379–394.
[3] V. Martin, P. Vignassa, Absorption d'une onde acoustique par les parois d'un guide 2D, *Journal de Physique IV, Colloque C1, supplément au Journal de Physique III* 2 (1992) 749–752.
[4] A. Cummings, Low frequency acoustic transmission through the walls of rectangular ducts, *Journal of Sound and Vibration* 61 (1978) 327–345.
[5] V. Martin, Perturbation of fluid-guided waves introduced by bending plates, *Journal of Sound and Vibration* 144 (1991) 331–353.
[6] A. Cummings, Stiffness control of low frequency acoustic transmission through the walls of rectangular ducts, *Journal of Sound and Vibration* 74 (1981) 351–380.
[7] R.J. Astley, A. Cummings, N. Sormaz, A finite element scheme for acoustical propagation in flexible walled ducts with bulk reacting liners, and comparison with experiment, *Journal of Sound and Vibration* 150 (1991) 119–138.
[8] F. Gautier, N. Tahani, Existence of two longitudinal guided waves in a fluid-filled cylindrical duct with vibrating walls, *Proceedings of Inter-Noise 96*, Liverpool, 30 July–2 August 1996.

[9] A. Cummings, R.J. Astley, The effects of flanking transmission on sound attenuation in lined ducts, *Journal of Sound and Vibration* 179 (1995) 617–646.
[10] A. Cummings, Sound transmission through duct walls, *Journal of Sound and Vibration* 239 (2001) 731–765.
[11] P.A. Nelson, S.J. Elliott, *Active Control of Sound*, Academic Press, London, 1992.
[12] V. Martin, V. Adam, M. Rossi, Predictive calculations for active noise control by anticipation and consequences of the violation of causality; numerical and experimental results, *Proceedings of Active 99*, Fort Lauderdale, FL, USA, 4–6 August 1999.
[13] R.J. Astley, Acoustical modes in lined ducts with flexible walls: a variational approach, *Proceedings of Inter-Noise 90*, 1990, pp. 575–578.
[14] D.E. Goldberg, *Genetic Algorithms in Search, Optimization, and Machine Learning*, Addison-Wesley, Boston, 1989.